Microfluid Nanofluid (2016) 20:12
DOI 10.1007/s10404-015-1668-z

RESEARCH PAPER

Axial orientation control of zebrafish larvae using artificial cilia

Chia-Yuan Chen[1] · Tsung-Chun Chang Chien[1] · Karthick Mani[1] · Hsiang-Yu Tsai[1]

Received: 9 June 2015 / Accepted: 20 October 2015 / Published online: 6 January 2016

Abstract Zebrafish has been used as an important vertebrate model of genetic screening and new drug development because of excellent characteristics, such as optical transparency, rapid ex vivo growth, and high genetic similarity to humans. Despite these advantages, studies on zebrafish are limited because of the lack of a robust and reliable method to manipulate zebrafish during microinjection and screening, as well as time-lapse imaging. In this work, a new microfluidic concept that utilizes a series of magnetically actuated artificial cilia integrated into a microchannel was employed to control the orientation of zebrafish larvae with a validated axial rotation capability. In contrast to conventional methods, the proposed method enables a highly accurate small-angle (0°–20°) stepwise axial rotation of a larva inside the microchannel with less detrimental effects on larval growth. The hemodynamics in a selected vessel was then imaged during the axial rotation of the tested larva to assist cardiovascular assessment. In addition, the bioactivity of the tested larvae remains stable without short-term negative effects after the imaging. The proposed platform, along with the provided analytical paradigm, can facilitate future zebrafish screening via microfluidics in the pharmaceutical industry.

Keywords Orientation control · Zebrafish · Artificial cilia · Microfluidics

Electronic supplementary material The online version of this article (doi:10.1007/s10404-015-1668-z) contains supplementary material, which is available to authorized users.

✉ Chia-Yuan Chen
chiayuac@mail.ncku.edu.tw

[1] Department of Mechanical Engineering, National Cheng Kung University, No. 1 University Road, Tainan 701, Taiwan

1 Introduction

The zebrafish has been recognized as an important animal model for biologists and engineers to investigate human diseases and is increasingly used in toxicological studies for new drug development (Chen and Cheng 2014). The popularity of zebrafish is attributed to its merits, which include skin transparency, high physiological growth rate, high degree of genetic similarity to mammals (Tamplin and Zon 2010), and ex vivo growth in aqueous medium (Chang et al. 2012). Also, large numbers of zebrafish are available to facilitate studies related to gene functions and the identification of cellular targets of new compounds (Chang et al. 2012). For instance, a recent study determined that a better understanding of the hemodynamics of zebrafish with Alk1 gene deficiency helped clarify the etiology of arteriovenous malformation, which is implicated in the human vascular disorder hereditary hemorrhagic telangiectasia type 2 disease (Chen et al. 2011). However, owing to the absence of a proper methodology in a zebrafish screening and imaging process, contemporary zebrafish tests can only be performed through a tedious and inefficient manual orientation control by an experienced operator. This poses a significant barrier to accelerate the progress of new drug development and gene screening processes where large quantities of zebrafish are usually required. Moreover, acute orientation adjustment is usually needed during imaging to identify the vessels or organs of interest. The accuracy of this operation is inevitably compromised by the limitations of manual control through forceps.

Recent trends are geared toward manipulating zebrafish embryos and larvae through microfluidic designs. Several novel microfluidic platforms have been demonstrated to successfully facilitate zebrafish manipulation in a more

automatic and robust fashion. For example, a microfluidic perfusion platform consisting of multiple inlets and outlets, a gradient generator, and a fish tank was presented to enable dose control of drugs on a chip (Choudhury et al. 2012). A microfluidic segment method using perfluoromethyldecalin as a carrier was employed to transport zebrafish embryos in a microchannel. Normal embryonic development of the tested embryo before hatching was observed inside the segment after the transport (Funfak et al. 2007). A microfluidic flow-through system was developed to facilitate automatic buffer removal during zebrafish imaging (Wielhouwer et al. 2011). A novel and practically advantageous high-throughput automatic zebrafish platform was applied, enabling a high degree of freedom in viewing angle alteration for in vivo screening. This platform is composed of an automatic embryo-loading section as well as a motorized capillary tube loaded with embryos (Pardo-Martin et al. 2010). Although the advances in the aforementioned microfluidic designs are beneficial for current in vivo screening for zebrafish, several improvements still need to be made before these presented platforms become commercially available. The main problem lies in a lack of a proper design to facilitate time-lapse imaging. Because of the rapid development of zebrafish, a beating heart and a functional circulatory system form within 26 h of fertilization and the heart develops into a two-chambered conformation within 48 h (Malone et al. 2007). A microfluidic design that can accommodate these drastic morphological changes in the zebrafish larvae during imaging is in high demand. A previously reported method for zebrafish immobilization during imaging through fluorinated ethylene propylene tubes (Kaufmann et al. 2012) is limited in this regard. This limitation is mainly because these capillaries or tubes are usually made in one size and is therefore incapable of adapting to the rapid shape change in zebrafish. In addition, this tubing-based system has no orthogonal dimensions available for coupling external chemical and physical stimuli, which limits their practicality for real-time recording of central nervous system (CNS) activities (Lin et al. 2014).

Driven by this motive, a strategy was put into practice through the idea of a fish trap. This was done through the immobilization of tested larval zebrafish in a trapping microchannel. The larval zebrafish was entrapped and restricted inside a microchannel right after released from a pipette. Additional access ports are available to administer chemicals, anesthetics, or treatments for the tested larva. A study demonstrated that a neutrophil migration screening test was conducted successfully with a microfluidic restriction array, and can be extended to study leukocyte motility and inflammation screening (Bischel et al. 2013). Internally dynamic responses of the larva under the treatment, such as neural and circulatory activities, can be recorded and quantified with the microfluidic trap (Lin et al. 2014). It shows that the local and global effects of pharmacoactive drugs on the nervous system can be visualized and analyzed through this trapping method, and the fabricated platform is also readily utilized for other external stimuli such as acoustic and optical signals. Although these methods sound promising, both of them are limited to the degree of freedom of altering the viewing angle during imaging. Imaged zebrafish larvae can only be viewed with four orthogonal viewing angles, namely ventral, dorsal, and two lateral views using the aforementioned methods. However, the complexity of zebrafish anatomy requires a highly precise orientation control to visualize a specific region of interest. For example, to assess the midline crossing of the Mauthner motor neuron axons that project into spinal cord, a specific angle observed from the hindbrain is required as the structure is obscured with other less favorable viewing angles (Pardo-Martin et al. 2010). Such phenotype evaluation plays a key component in facilitating zebrafish screening studies for new drug development. In this study, a zebrafish manipulation concept was initiated by integrating a series of artificial cilia into the microchannel to facilitate the visualization of zebrafish phenotypes. To the authors' understanding, this is the first attempt to provide axial orientation control of zebrafish larvae through artificial cilia actuation.

2 Materials and methods

2.1 Zebrafish preparation and high-speed fluorescent image acquisition

Wild-type and transgenic *Tg*(*gata1:DsRED*) zebrafish (*Danio rerio*) were incubated and raised at 28 °C according to standard protocols (Chen et al. 2011). This transgenic line expresses red fluorescent protein (DsRED) signal from blood cells. Zebrafish larvae were anesthetized with tricaine for 3 min before axial rotation and high-speed recording. Two separate anesthetic dosages (0.091 and 0.154 mg/mL) were selected for treatment based on the responses of the test larva. If the tested larva still shows an active behavior after taking the lower dosage treatment (0.091 mg/mL), the larva will be subject to a higher dosage treatment (0.154 mg/mL) before loading into the microchannel for orientation control. Tested larvae are in a stage with length values between 4.0 and 4.2 cm. The high-speed recording was done through a fluorescent microscope (BX60, Olympus Corp., Japan) connected to a high-speed camera (NR4-S2, IDT, Tallahassee, FL, USA) with a frame rate of up to 2000 Hz at a resolution of 1024 × 1024 pixels. Time-dependent kinetics of larval zebrafishes as well as artificial cilia inside the microchannel were analyzed and

quantified using the motion analysis software DLT Dataviewer (Hedrick 2008).

2.2 Fabrication of the artificial cilia embedded microchannel

Axial rotation of larval zebrafishes was achieved through the actuation of a series of artificial cilia embedded inside the microchannel in a concerted fashion. A microfabrication process was employed to fabricate the artificial cilia. This process started with a micromilling step where a straight microchannel mold was carved onto an acrylic substrate. The microchannel was designed to measure 580 μm in width and 1.5 mm in depth to accommodate both the zebrafish larvae and artificial cilia. To fabricate the artificial cilia, microholes with 250 μm in diameter and 1.0 mm in depth were drilled from the microchannel mold, and subsequently, artificial cilia composite was poured into these microholes. The artificial cilia composite consisted of commercially available 5 μm in diameter neodymium–iron–boron magnetic particles (MQP-15-7, Magnequench, Singapore) and polydimethylsiloxane (PDMS, Sylgard 184, Dow Corning Corp., Midland, MI, USA) with a weight ratio of 4–1. The hole filling with composite mixture requires the filling step for multiple times until the composite is entirely filled up the holes. Once the filling of the holes was completed, the entire mold was filled with degassed PDMS solution followed by a curing process, which involved a hotplate baking step at 95 °C for 48 h for the solidification of both the composite and the filled PDMS solution. The final two steps included the mold removal from the duplicated PDMS-based microchannel and the opening enclosure along with tubing connection for zebrafish loading and discharging. The top opening of the microchannel was sealed with a glass cover slip through oxygen plasma treatment (Harrick Plasma Inc., Ithaca, NY) for 3 min at the RF power of 18 W. The tubing connection for zebrafish loading and discharging was achieved by squeezing the tubing with 1.5 mm in diameter into the side opening of the microchannel, and a drop of partially cured PDMS solution was employed as an adhesive layer added in the vicinity of the junction between the tubing and the side opening. Schematic illustrations of the fabrication process flow and the experimental setup for the fabricated microchannel with artificial cilia embedded are shown in Fig. 1.

2.3 Magnetic field control

In the actuation of artificial cilia, a homogeneous magnetic field is required to be accurately generated. Therefore, an in-house magnetic coil system was developed and demonstrated. A data acquisition device (NI cDAQ-9174, National Instruments, Austin, TX, USA) with modules embedded for signal inputs and outputs (NI 9201 and 9264) was used to provide a link between the magnetic coil and a power supply (GPR-3510HD DC Power Supply, Instek, Taiwan). An in-house script was also implemented in the proposed control algorithm via a graphical user interface (Fig. 2a, b) of the data acquisition device. In the control algorithm, a square wave was selected as a modulated signal to control the current supplied to the coil to generate the magnetic field. This square wave has a high level of 5 V and a low level of 0 V with the switching frequency of 240 Hz which was treated as a switch that allows the current to pass through. The total current supply to the coil is higher when the time at which the switch is on is longer than the time at which the switch is off. With this configuration, the proposed magnetic coil system can cause the artificial cilia to generate diversely beating behaviors, such as circular, half-circular, and back-and-forth moving trajectories. In this work, only the data using the back-and-forth beating behavior were recorded. The coil set was assembled using the following procedures. The magnetic coil consisted of an iron hexagon bar (0.6 cm on each side) wrapped with a 24-gauge single-strand magnetic coil at 1055 turns. To quantify the strength of the generated magnetic field through the magnetic coil system, a Hall effect sensor (A3503, Allegro MicroSystems, LLC, Worcester, MA, USA) with various duty cycles of the coil set was employed. The results showed that the generated magnetic field increases linearly as the duty cycle of the square wave increases (Fig. 2c). The direct link between the artificial cilia actuation and the duty cycle is further given in Fig. 2d where the tilting angle (with respect to the microchannel bottom wall) increases linearly with the increase in duty cycle. This feature is important for axial orientation control of the zebrafish as the linear stepwise function is applicable through the change in duty cycle. In this design, only one magnetic coil was used. The proposed magnetic coil system can also trigger and control at least four magnetic coils; each magnetic coil displays a 90° separation angle on the horizontal plane to enhance the controllability. A fully automated zebrafish loading and unloading design can be implemented in the current configuration to expedite the zebrafish imaging.

2.4 Axial rotation tests and measurement

The zebrafish larvae were axially rotated to accurately control the orientation of the zebrafish. The axially rotational movement was quantified by determining the projected change in the body shape of the tested larvae. The projected change in the body shape was calculated by measuring the distance of two specific body features projected on the imaging plane during rotation. The three sets of distance

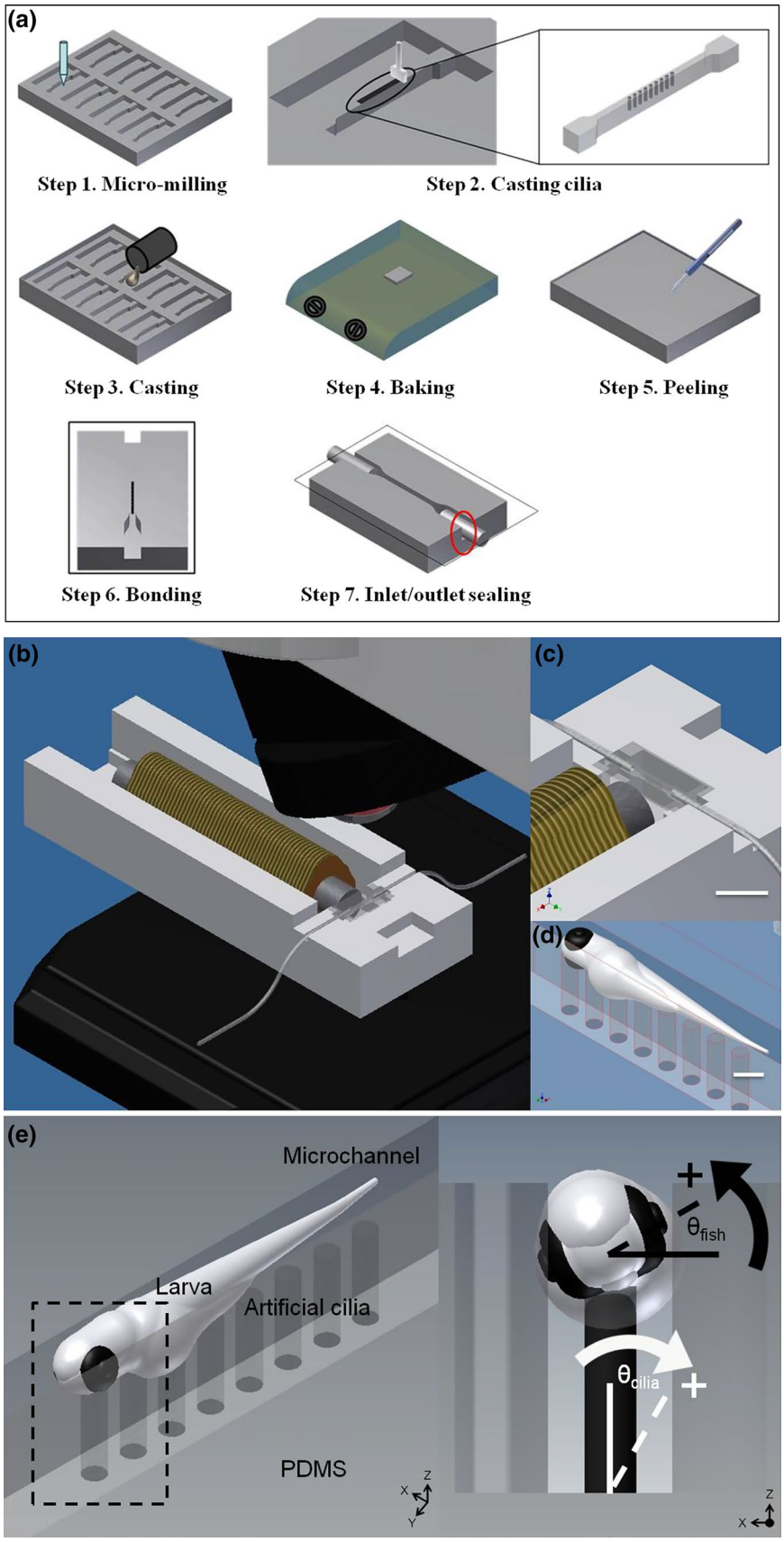

Fig. 1 Fabrication of the zebrafish orientation control platform. **a** A micromachining method was used to determine the geometric features of the platform. **b** Assembled platform with an integrated magnetic coil. **c**, **d** Zoom-in images of the platform with embedded artificial cilia. *Scale bar* 11 mm (**c**) and 0.55 mm (**d**). **e** Angle definitions for both artificial cilia and the larval zebrafish during the axial rotation control. The zebrafish rotates counter-clockwise in response to the clockwise rotation of artificial cilia

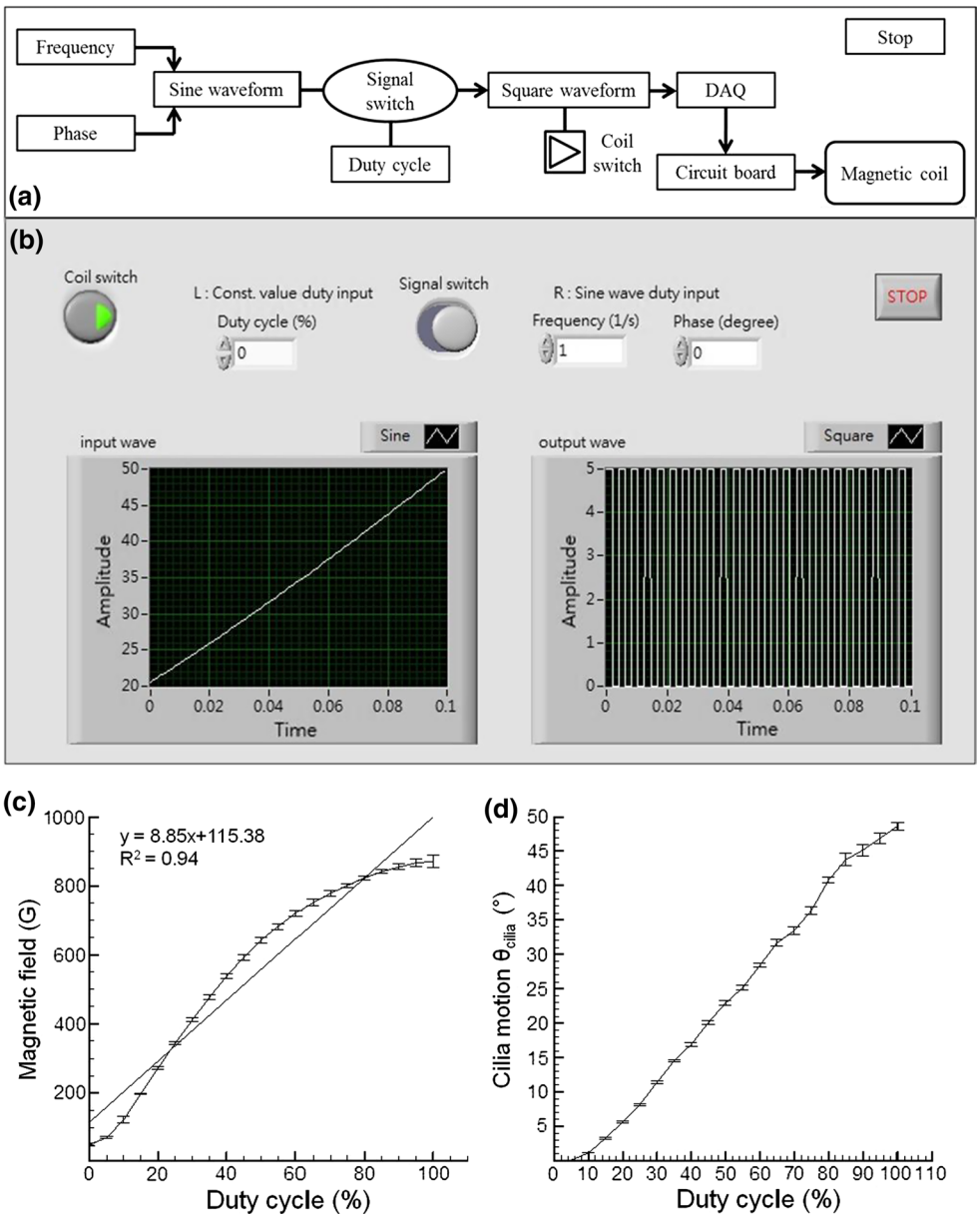

Fig. 2 Magnetic field control algorithm (**a**) and user interface control panel (**b**) for the stepwise axial control of the zebrafish larvae inside a microchannel through the artificial cilia actuation. The percentage of a square wave period when a signal stays active is determined by the duty cycle (from 0 to 100 %). **c** Changes in the generated magnetic field in response to the change in the duty cycle. This measurement was conducted at an operating voltage of 6 V supplied to the Hall effect sensor. **d** Relationship between the tilting angle of artificial cilia and the duty cycle

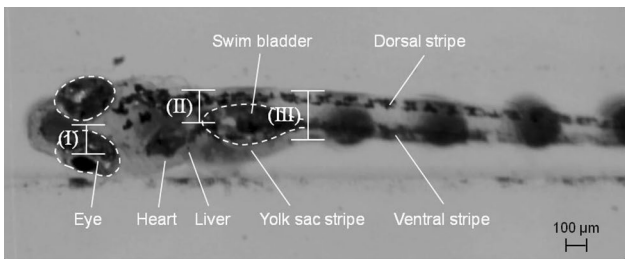

Fig. 3 Quantification of the axial rotation of zebrafish larvae by determining the changes in the distance of the projected body features

changes, including lines I, II, and III, were determined (Fig. 3). Line I is the shortest vertical distance between the body midline and the left eye center. Line II is the shortest vertical distance between the boundary of the dorsal stripe and the proximal side of the swim bladder. Line III is the body width of the trunk (next to the distal end of the bladder). A series of image preprocessing algorithms, such as contrast enhancement and noise reduction, was applied before these projected changes in the distance were calculated. The proposed quantification method of the changes in distance was conducted semi-automatically. Once the projected change in the distance was measured, a cosine relation formula was used to quantify the relative angle change (with respect to the original orientation) in the tested larvae.

An additional test was conducted to analyze motion by using an open source code Tracker (Brown 2013) and to validate the proposed quantification method. The projected

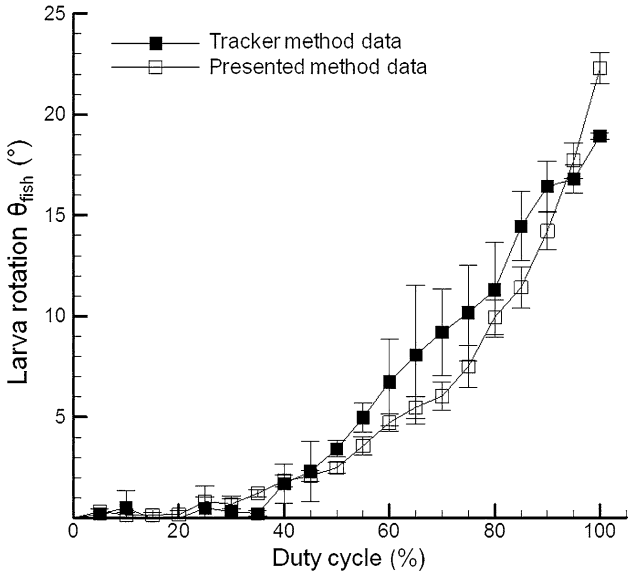

Fig. 4 Changes in the distance in line II during the axial rotation of the zebrafish larvae were measured and compared using the proposed method and the open source motion analysis code to validate the results. Each data point was determined five times for the same larva; statistic information such as average and one standard deviation is provided

change in the distance of line II during the axial rotation of the zebrafish larvae was measured and compared using the proposed method and the Tracker. The results of both methods showed consistent patterns of the duty cycle from 0 to 100 % with an apparent deviation only at the duty cycle of 100 % (Fig. 4). This result demonstrated that the proposed method is reliable, robust, and capable of small-angle motion quantification. In the early phases of axial rotation (duty cycle below 40 %), flat curves are identified because the overall rotational angle is <2°. For rotational angles with a duty cycle of ≥40 %, the larval rotation is strongly and linearly correlated with duty cycle. In addition to body feature tracking, correlation coefficient calculation (Chen et al. 2014) was performed on the basis of the recorded zebrafish image sets during axial rotation; thus, a secondary validation of the angle measurement was achieved in terms of the degree of image similarity. The correlation coefficient was calculated by comparing the rotated zebrafish images with the unrotated zebrafish image. Indeed, the rotating angle can be statistically verified on the basis of correlation coefficients.

3 Results and discussion

3.1 Axial rotation of zebrafishes using artificial cilia

A series of artificial cilia was employed as an actuator to axially rotate the zebrafish larvae for stepwise rotational angle manipulation. The rotation process and the results are described as follows. The artificial cilia were not actuated until the tested larvae settled on top of the inner artificial cilia of the microchannel. Stepwise rotation was performed through the direct contact of the artificial cilium tips and the larval body when the artificial cilia were in motion. No translational motion can be achieved for the larvae under this condition because the space is limited inside the microchannel. Therefore, the larvae were forced to rotate axially in response to the movement of the artificial cilia. The relationship between the relative rotation angle and the applied magnetic field (denoted as duty cycle) is shown in Fig. 5a. In general, a large duty cycle corresponds to a great magnetic field; therefore, the tilting angle range of each artificial cilium is wide. This condition increases the degree of the axial rotation of the zebrafish larvae (with respect to the orientation of the larva before rotation). However, the orientation of each larva is slightly different from one another right after each larva is loaded into the microchannel with a fixed width (580 μm in this case); the rotation angle was assumed as zero when the duty cycle was 0 % in each larva test. On the basis of this assumption, we calculated the

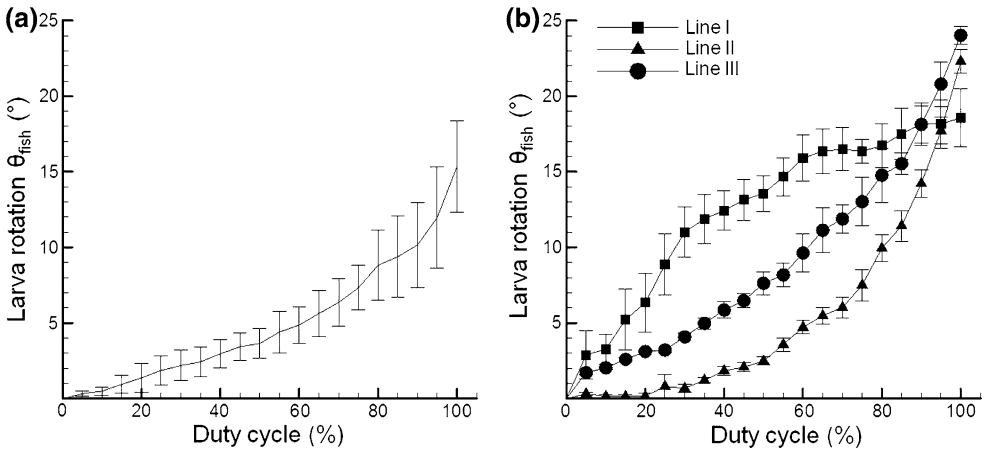

Fig. 5 Stepwise axial rotation of the zebrafish larvae through artificial cilium actuation. **a** Changes in the measured larval rotational angle in response to the change in the duty cycle of the magnetic coil. Line II was determined to provide the rotational angle; eleven zebrafish larvae were evaluated and summarized. **b** Quantitative angle measurement against duty cycle was performed in three different measurement locations of a selected larva

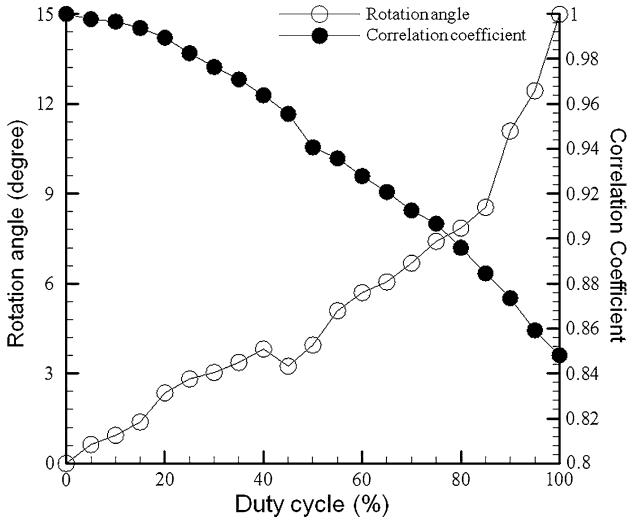

Fig. 6 Stepwise axial rotation patterns of a selected zebrafish larva through artificial cilia actuation in different duty cycles; rotation angles were evaluated using the cosine relation formula, and the correlation coefficient values were calculated to provide information on image similarity

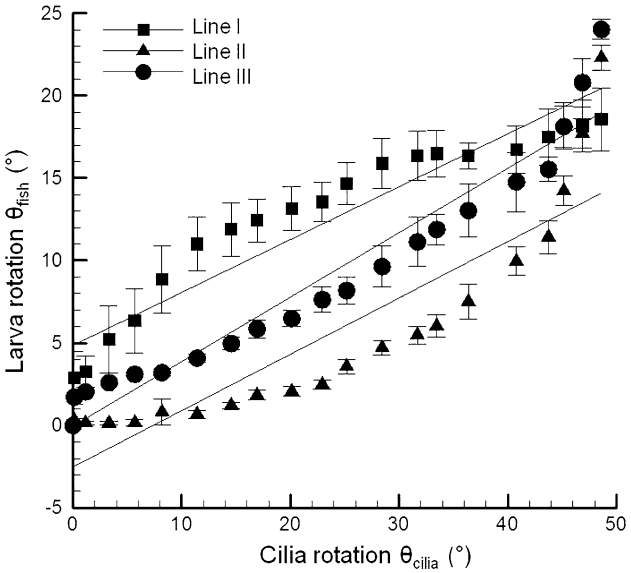

Fig. 7 Quantification of the relative motion between the artificial cilia and the tested zebrafish larvae. Changes in the rotational angle of the tested larva in response to the artificial cilia actuation in three different tested locations. *Solid lines* represent the linear fitting results of the three measured curves. R^2 of the three curves was >0.8

rotational angle at different duty cycles. The test results of 11 larvae were collected, and the variations of the measured rotation angles in each duty cycle were estimated as <20 %. This test aimed to develop a very fine step of angle adjustment in the range between 0° and 20°; therefore, this 20 % variation is acceptable. In addition, rotational angles at three locations of body features, namely lines I, II, and III, were quantified and plotted against the duty cycle to determine whether the passage of the axial rotational motion is distributed uniformly through the trunk of the tested larvae or only a specific part of the body can be actuated locally (Fig. 5b). The three curves, which represent the angle measurement results at the proximal, middle, and distal sections of the larva during artificial cilium cilia, increase linearly and uniformly as duty cycle increases. Nevertheless, deviations among the three curves are observed. The obtained discrepancy is attributed to the variations of the local stiffness of the body surface in contact with the artificial cilia. Such stiffness difference affects the local rotation of the larvae. Despite these findings, the overall controllability of the proposed method is reliable and robust in terms of the rotational control of the larval motion; this result is supported by the three curves that show a consistent trend.

In addition to the relative rotational angles evaluated using the cosine relation formula, the correlation coefficients were calculated from the rotating zebrafish images to provide a secondary alternative to quantify axial rotation. A larva was selected and rotated using the underlying artificial cilia (Fig. 6). The angle rotation results calculated using the cosine relation and the correlation coefficients are presented. The results of these two methods are consistent. In general, a high correlation coefficient corresponds to a high degree of similarity between the two calculated images of the larva during rotation. Therefore, the peak correlation coefficient (value = 1) is obtained when the rotational angle is zero (duty cycle = 0) because the two obtained images are identical. This value decreases as duty cycle increases because the image of the rotated larva with a higher degree is less similar to the image before the larva is rotated; this finding is consistent with the results calculated using the cosine formula. The consistent results of both methods demonstrated that the proposed method with artificial cilium actuation can accurately perform small-angle axial rotation.

3.2 Quantification of relative motion of larval zebrafishes during artificial cilia actuation

The relative axial rotation of larval embryos during artificial cilia actuation was quantified (Fig. 7) by plotting the change in the rotational angle of the larva against the tilting angle of the artificial cilia. The images along the *x*–*y* plane with the tested larva placed on top of the artificial cilia were recorded in this test; in this figure the rotational movements can be controlled accurately through the small increments of the tilting angle of the artificial cilia. This finding is evidenced by a high degree of linearity with R^2 of >0.8 between the rotational motions of the larva and the artificial cilia; this degree was calculated in three different

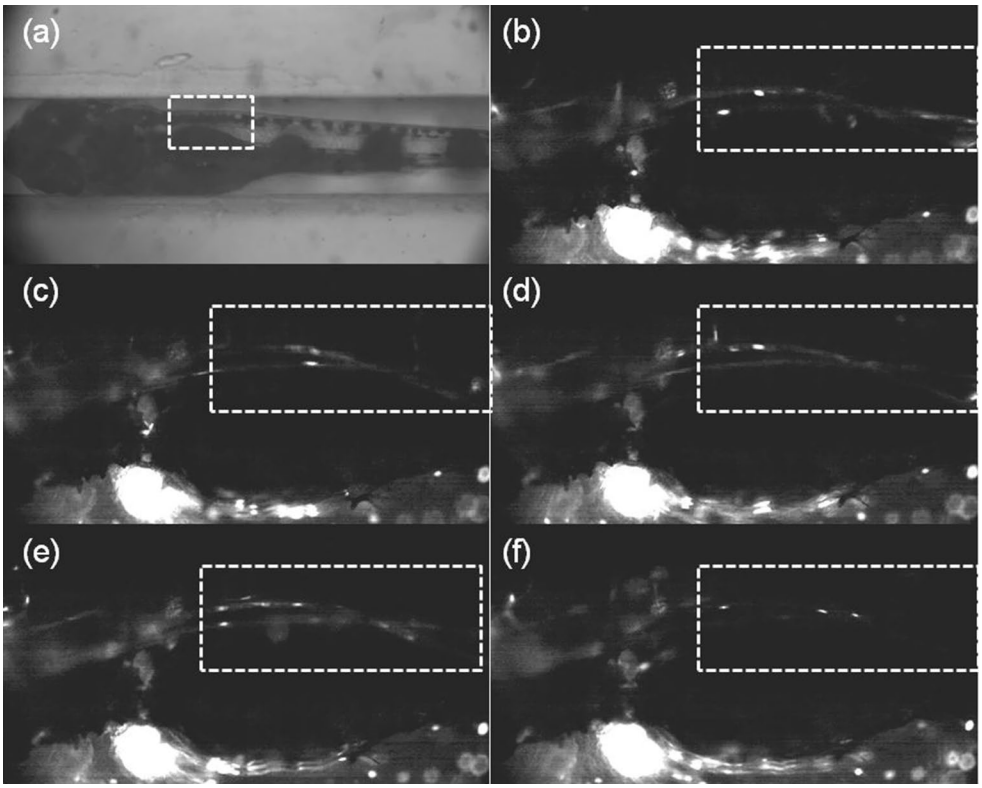

Fig. 8 Snapshots of the larval zebrafish during the axial rotation using artificial cilia. **a** An optical microscope image at the magnification of 50×. **b–f** Fluorescent images (20×) showing the DsRED signals from the blood cells inside the larva with duty cycle of 0 % (**b**), 20 % (**c**), 40 % (**d**), 60 % (**e**), and 80 % (**f**). The *dashed white rectangle* highlights the region of interest where both the dorsal aorta (*upper vessel*) and the posterior cardinal vein (*lower vessel*) go from appearing to vanishing on the image plane when the duty cycle increases from 0 to 80 %

changes in the body feature of the larva (lines I to III). Therefore, stepwise rotational movement can be achieved with the presented experimental paradigm. Nevertheless, the three curves do not overlap with one another; this finding indicates that the passage of the actuated axial rotation is not perfectly uniform along the body of the larva even with a series of artificial cilia moving in a concerted fashion. To solve this problem, sequential tilting of the artificial cilia should be performed which requires a more sophisticated configuration in terms of magnetic field control. Although the results are not shown, the proposed method can be used to rotate the zebrafish clockwise and counterclockwise in a stepwise manner. This feature is practically advantageous to provide quantitatively hemodynamic results to investigate angiogenesis; this advantage is possible because the local three-dimensional reconstruction of blood vessels can be achieved. With this reconstruction, shear stress can be accurately calculated through the enabled bilateral rotation movement of the tested larva via artificial cilia actuation. However, the current design is also limited because a 360-degree rotation cannot be achieved at high accuracy.

3.3 In vivo axial rotation test

It has been a challenge to achieve stepwise orientation control using manually controlled forceps in a regular in vivo imaging. The presented method pushed one step further by adapting the morphological change in larva during growth (the presented device is suitable for larval fishes with 4.0–4.2 cm in length) to the stepwise rotational control. To demonstrate that this method is practical, two vessels of a larval zebrafish were imaged during the axial rotation. In Fig. 8, both the dorsal aorta (upper vessel) and the posterior cardinal vein (lower vessel) are in the highlighted region (white dashed rectangle) that was selected as the region of interest. However, the posterior cardinal vein is not visible when the duty cycle is 0 % (no rotation). Both the vessels are not clearly visible until the duty cycle was increased to over 20 %, and the most favorable visible scene was chosen when the duty cycle is 60 %. Further increasing the duty cycle to 80 % results in a blurry image. Therefore, the presented method enables small-angle axial rotation that facilitates the screening of zebrafishes with a higher degree of viewing angles than previous published methods.

4 Conclusions

A first successful attempt of manipulating the orientation of zebrafish larvae through the underlying artificial cilia actuation was demonstrated to provide a robust platform for biological screening. Through the presented microfluidic paradigm, larvae with size differences in a certain range can be rotated axially with high accuracy in a stepwise manner. This feature is beneficial for time-lapse imaging. Integration of additional access ports to the current design is also possible for chemical injections of larvae. Altogether, an orientation control platform was developed for diverse biomedical assays that is robust, has a high degree of orientation control, and has a less detrimental impact on in vivo screening.

Acknowledgments This study was supported by Ministry of Science and Technology of Taiwan under Contracts Nos. MOST 104-2221-E-006-169 and MOST 102-2221-E-006-297-MY3 (to Chia-Yuan Chen). This work would not be possible without the facility provided by Center for Micro/Nano Science and Technology, National Cheng Kung University. The research was in part supported by the Ministry of Education, Taiwan, R.O.C., through the Aim for the Top University Project to National Cheng Kung University (NCKU).

References

Bischel LL, Mader BR, Green JM, Huttenlocher A, Beebe DJ (2013) Zebrafish Entrapment By Restriction Array (ZEBRA) device: a low-cost, agarose-free zebrafish mounting technique for automated imaging. Lab Chip 13:1732–1736

Brown D (2013) Sharing video experiments with tracker digital libraries paper presented at the American Association of Physics Teachers, AAPT, New orleans, Louislana

Chang TY, Pardo-Martin C, Allalou A, Wahlby C, Yanik MF (2012) Fully automated cellular-resolution vertebrate screening platform with parallel animal processing. Lab Chip 12:711–716

Chen CY, Cheng CM (2014) Microfluidics expands the zebrafish potentials in pharmaceutically relevant screening. Adv Healthc Mater 3:940–945

Chen CY, Patrick MJ, Corti P, Kowalski W, Roman BL, Pekkan K (2011) Analysis of early embryonic great-vessel microcirculation in zebrafish using high-speed confocal muPIV. Biorheology 48:305–321

Chen CY, Anton R, Hung MY, Menon P, Finol EA, Pekkan K (2014) Effects of intraluminal thrombus on patient-specific abdominal aortic aneurysm hemodynamics via stereoscopic particle image velocity and computational fluid dynamics modeling. J Biomech Eng 136:031001

Choudhury D et al (2012) Fish and chips: a microfluidic perfusion platform for monitoring zebrafish development. Lab Chip 12:892–900

Funfak A, Brosing A, Brand M, Kohler JM (2007) Micro fluid segment technique for screening and development studies on Danio rerio embryos. Lab Chip 7:1132–1138

Hedrick TL (2008) Software techniques for two- and three-dimensional kinematic measurements of biological and biomimetic systems. Bioinspir Biomim 3:034001

Kaufmann A, Mickoleit M, Weber M, Huisken J (2012) Multilayer mounting enables long-term imaging of zebrafish development in a light sheet microscope. Development 139:3242–3247

Lin X et al (2014) High-throughput mapping of brain-wide activity in awake and drug-responsive vertebrates. Lab Chip 15:680–689

Malone MH, Sciaky N, Stalheim L, Hahn KM, Linney E, Johnson GL (2007) Laser-scanning velocimetry: a confocal microscopy method for quantitative measurement of cardiovascular performance in zebrafish embryos and larvae. BMC Biotechnol 7:40

Pardo-Martin C, Chang TY, Koo BK, Gilleland CL, Wasserman SC, Yanik MF (2010) High-throughput in vivo vertebrate screening. Nat Methods 7:634–636

Tamplin OJ, Zon LI (2010) Fishing at the cellular level. Nat Methods 7:600–601

Wielhouwer EM et al (2011) Zebrafish embryo development in a microfluidic flow-through system. Lab Chip 11:1815–1824